Macromolecules
COMMUNICATION TO THE EDITOR

Macromolecules **2010**, *43*, 3173–3176 **3173**
DOI: 10.1021/ma100044q

Percolation-Driven Multiscale Roughening for Superhydrophobic Polymer Nanocomposite Coatings

Shane E. Harton,*,† Cynthia G. Templeman,‡ and Brenda Vyletel§

†*Materials Research Department, Toyota Research Institute of North America, Toyota Technical Center, Ann Arbor, Michigan 48105,* ‡*Materials Engineering Division, Toyota Technical Center, Ann Arbor, Michigan 48105, and* §*Electron Microbeam Analysis Laboratory, University of Michigan, Ann Arbor, Michigan 48109*

Received January 7, 2010
Revised Manuscript Received March 5, 2010

Controlling wettability by chemically and physically tailoring surfaces is a well-established field of research.[1,2] Advances in technologies surrounding wetting, superhydrophobicity, and superoleophobicity have been rapid in recent years due to the numerous applications such as microfluidics and antifogging, self-cleaning, and antifouling surfaces and coatings.[3−9] Creating superhydrophobic surfaces often involves mimicking the naturally occurring Lotus leaf, a well-known symbol of purity due to its self-cleaning capabilities.[10] The Lotus leaf is superhydrophobic due to its surface chemistry and surface morphology.[3] Multiscale surface roughness partially excludes water at the three-phase contact line formed at the water/surface/air interface (i.e., the meniscus),[5] resulting in water contact angles (WCA's) much greater than with a smooth analogue. Nature has created such surfaces with other plants, such as the Indian Cress and Lady's Mantle,[10] and in insects, such as the legs of a water strider.[3] It is therefore logical to artificially mimic something that nature has perfected so many times when designing superhydrophobic surfaces.

One practical method for artificially mimicking the Lotus leaf involves incorporating hydrophobic nanoparticles into a polymer matrix.[11,12] This technique provides a versatile method for coating substrates of various sizes, geometries, and surface chemistries.[5] A simple processing step that facilitates uniformity and reproducibility of polymer nanocomposite properties from sample to sample involves thermally equilibrating the sample.[13] However, we have been able to determine, through simple theoretical analysis, that the thermodynamic forces that drive hydrophobic nanoparticles to polymer surfaces during thermal annealing are not strong enough to cause significant roughening.

Here, theoretical predictions have been experimentally verified with nanocomposite coatings at low nanoparticle concentrations. It is further demonstrated at higher nanoparticle concentrations that thermally equilibrated polymer nanocomposites must percolate in order to become superhydrophobic, with the observation of a distinct transition in WCA's from hydrophobic (∼100°) to superhydrophobic (>150°) above the percolation threshold. Long-range assembly of the nanoparticles is therefore the dominant driving force for formation of multiscale roughness at the surface of the polymer nanocomposites (i.e., Lotus effect) and, hence, superhydrophobicity.

The nanocomposite system used here is composed of a polystyrene (PS) matrix and polydimethylsiloxane (PDMS) coated pyrogenically prepared (fumed) silica (PDMS−SiO_x) nanoparticles. The PDMS−SiO_x primary particle diameters are ∼20 nm, and primary aggregate lengths are ∼100 nm, as determined using transmission electron microscopy (TEM). Elemental analysis was used to approximate a surface coverage of 1.6 ± 0.3 mg/m^2 of irreversibly physisorbed PDMS,[14] which is equivalent to an effective thickness ∼2 statistical segment lengths. Therefore, the matrix polymer will not directly interact with the silica surface. Two different 200 kDa PS samples were used, with one having a narrow molecular weight distribution (PS-ND) and the other having a broad molecular weight distribution (PS-BD). Both have glass transition temperatures ≈100 °C. PS was dissolved in chloroform ($CHCl_3$), and PDMS−SiO_x was dispersed separately in $CHCl_3$. Particle suspensions were bath-sonicated for 20 min, and then polymer and particle solutions were combined and vigorously shaken for 1 h followed by sonication for 10 min. Nanocomposite suspensions were drawn-down onto aluminum substrates with resulting dry films ∼20 μm thick. Suspensions were also solution-cast into PTFE (Teflon) dishes for analysis of the bulk morphology using TEM. Nanocomposites and pure PS coatings were annealed for 72 h at 160 °C under argon in a glovebox (<0.1 ppm of O_2). No changes in WCA's were observed after 24 h annealing. Samples were analyzed using contact angle goniometry, atomic force microscopy (AFM), field-emission scanning electron microscopy (FE-SEM), X-ray photoelectron spectroscopy (XPS), TEM, and Knoop hardness measurements. See Supporting Information for more details regarding materials, sample preparation, and analysis.

The contact angle formed between a liquid and a solid substrate for homogeneous smooth surfaces can be related to the surface and interfacial free energies by the Young equation[15]

$$\cos\theta_l = \frac{\gamma_s - \gamma_{sl}}{\gamma_l} \tag{1}$$

where θ_l is the liquid contact angle (91° for water on glassy PS),[16] γ_s is the surface energy of the solid surface (42 mJ/m^2 for glassy PS),[16] γ_l is the surface energy of the liquid (72.8 mJ/m^2 for water),[16] and γ_{sl} is the liquid/solid interfacial energy. This equation has been modified for rough and/or chemically heterogeneous surfaces by Wenzel[17] and by Cassie and Baxter.[18] There has been some controversy over the Wenzel, and Cassie and Baxter interpretations of the Lotus effect in recent years;[19,20] however, as will be shown in this paper, neither interpretation would provide any further insight into the physical driving force behind superhydrophobicity with thermally equilibrated polymer nanocomposites, that is, percolation-induced hierarchal roughness. Equation 1 has been rearranged (see Figure 1a) using the relationship between polymer melt/particle contact angle (θ_m) and the equilibrium height the nanoparticle protrudes normal to the polymer melt surface (h_{eq})

$$\frac{h_{eq}}{R} = 1 + \frac{\gamma_{pm}}{\gamma_m} - \frac{\gamma_p}{\gamma_m} \tag{2}$$

where R is the particle radius, γ_{pm} is the particle/melt interfacial energy, γ_p is the particle surface tension (23 mJ/m^2 for physisorbed PDMS),[16] and γ_m is the polymer melt surface tension (31 mJ/m^2 for PS at 160 °C).[21] Increasing γ_{pm}, and hence the incompatibility between the particle and polymer matrix, and decreasing γ_p favor particle protrusion, a rather intuitive conclusion.

*To whom correspondence should be addressed. E-mail: shane.harton@gmail.com.

Published on Web 03/10/2010

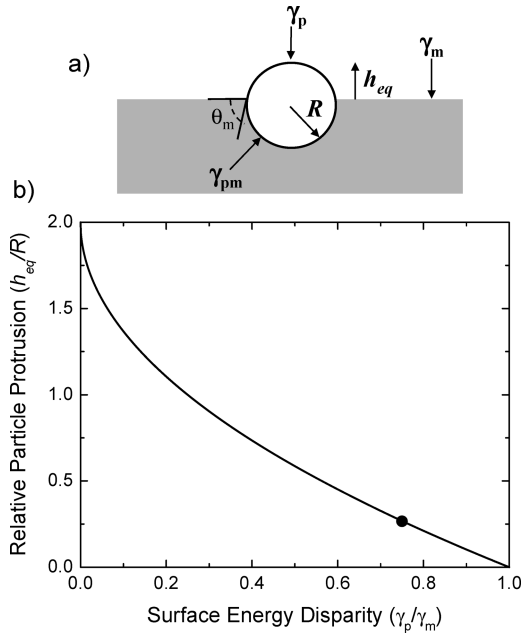

Figure 1. (a) Depiction of equilibrium protrusion (h_{eq}) of a spherical nanoparticle at a polymer melt surface. (b) Relative particle protrusion heights (h_{eq}/R) as a function of surface energy disparities (γ_p/γ_m). The filled circle (●) shows the equilibrium protrusion height for the system used here ($\gamma_p/\gamma_m \approx 0.75$). Equation 3 predicts that PDMS−SiO_x nanoparticles will only protrude the PS coating surface ~30% of the particle radius at 160 °C.

Using the geometric mean approximation,[15] eq 2 can be further simplified

$$\frac{h_{eq}}{R} \sim 2\left(1-\sqrt{\frac{\gamma_p}{\gamma_m}}\right) \quad (3)$$

Equation 3 provides a simple way to theoretically approximate the relative particle protrusion height (h_{eq}/R) as a function of surface energy disparity (γ_p/γ_m) only. See Supporting Information for more details regarding eqs 2 and 3. It should be noted that eqs 2 and 3 do not fully capture the overwhelming complexities of real polymer nanocomposites.[22,23] Nanoparticles tend to have a broad distribution of sizes and are rarely perfectly spherical, particularly for very small particles (< 50 nm diameter). Also, hydrophobic nanoparticles tend to be incompatible with polymer coatings, resulting in particle aggregates rather than isolated, well-dispersed particles. The PDMS−SiO_x particles used here are actually aggregated (fused) during synthesis (see Supporting Information). However, eqs 2 and 3 still illustrate the energetic competition between minimizing the contact area between the nanoparticles and polymer matrix and increasing the surface area upon nanoparticle protrusion through the coating surface, thereby providing physical insight into these complex systems by outlining the weak thermodynamic forces driving surface segregation. Figure 1b shows the predicted values for h_{eq}/R as a function of γ_p/γ_m using eq 3 and the predicted equilibrium protrusion height for the system used here ($\gamma_p/\gamma_m \approx 0.75$). Equation 3 predicts that the PDMS−SiO_x nanoparticles will only protrude the PS melt surface by about 30% of the radial height ($h_{eq}/R \sim 0.3$) at 160 °C. In fact, for a particle to protrude an entire hemisphere ($h_{eq}/R = 1$), γ_p/γ_m has to be ~1/4, a significant disparity in surface energies between particle and polymer.

Clearly, the thermodynamic driving forces alone are not enough to create the level of roughness necessary to make the nanocomposite surfaces superhydrophobic through the Lotus effect.[2,3] However, Figure 2a shows that the annealed PS/PDMS−SiO_x

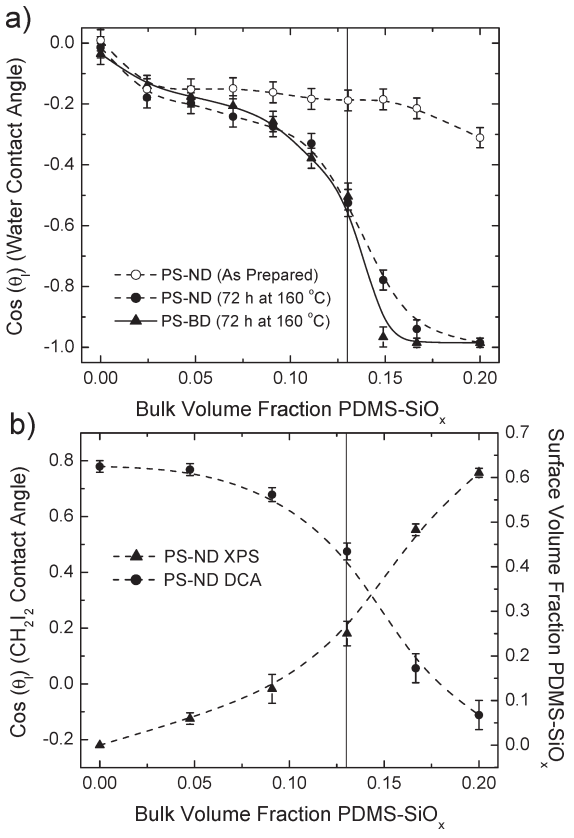

Figure 2. (a) Water contact angles for PS−ND nanocomposites as-prepared (○), PS−ND nanocomposites after 72 h at 160 °C (●), and PS−BD nanocomposites after 72 h at 160 °C (▲). Both of the thermally equilibrated systems have a sharp transition at ~13 vol % PDMS−SiO_x (shown with vertical line), but this transition is not apparent in the as-prepared samples. (b) Diiodomethane contact angles (●) and surface volume fractions of PDMS−SiO_x approximated from XPS (▲) for thermally equilibrated PS−ND nanocomposites. Note the transition in both DCA's and surface volume fractions at ~13 vol % PDMS−SiO_x (shown with vertical line). Lines are a guide for the eye.

nanocomposites become superhydrophobic above ~13 vol % particle loading, with an identifiable transition in WCA's. This is not a consequence of surface topography created during sample preparation because the as-prepared (dried for 24 h at room temperature in an ambient environment) samples are not superhydrophobic at any nanoparticle concentration (WCA's < 110°). A comparison of the WCA's for the thermally equilibrated PS−ND and PS−BD nanocomposites in Figure 2a shows excellent reproducibility. It should also be noted that water roll-off occurs at tilt angles ≪10° for 17 and 20 vol % PDMS−SiO_x concentrations with both the PS−ND and PS−BD nanocomposites (after annealing), implying low contact angle hysteresis (i.e., stable superhydrophobicity).[3,8,9,12] XPS was used to quantify the atomic fractions of carbon, silicon, and oxygen within a sampling depth ~5−10 nm of the annealed PS−ND nanocomposite surfaces, and from this, the effective surface volume fractions of PDMS−SiO_x were approximated (see Figure 2b). Results at lower filler concentrations (< 13 vol %) show surface concentrations of PDMS−SiO_x similar to the bulk concentrations, which is indicative of weak thermodynamically driven surface segregation. Above 13 vol % surface segregation of PDMS−SiO_x is greatly enhanced, with ≈60 vol % PDMS−SiO_x at the surface for 20 vol % bulk concentration.

Diiodomethane (CH_2I_2) contact angles (DCA) are also shown in Figure 2b. Diiodomethane has an affinity for PS[24] ($\theta_l = 35$ and $\gamma_l = 50.8$ mJ/m^2)[16] and could become superamphiphilic on rough PS surfaces.[3] Below 13 vol % PDMS−SiO_x, the DCA's are

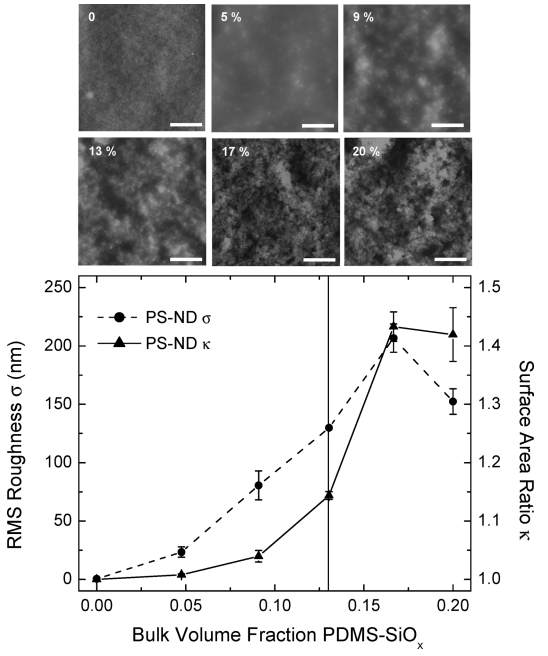

Figure 3. AFM images (top) for PS−ND nanocomposites after 72 h at 160 °C and resulting root-mean-square (rms) roughness values (bottom, ●) and ratios of the topographical surface area to the projected surface area (bottom, ▲). The vertical line represents the approximate transition concentration from WCA measurements (~13 vol % PDMS−SiO_x) shown in Figure 2. The scale bars in the AFM images represent 5 μm. Lines are a guide for the eye.

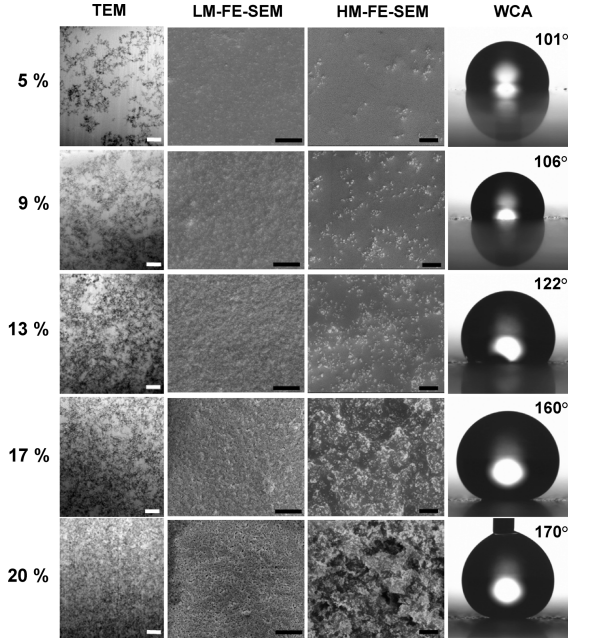

Figure 4. TEM images of the bulk PS−ND nanocomposites, low magnification (2500×) and high magnification (35000×) FE-SEM images (LM-FE-SEM and HM-FE-SEM, respectively) of the PS−ND nanocomposite surfaces and corresponding WCA images of the PS−ND nanocomposite surfaces (all samples were annealed at 160 °C for 72 h). The scale bars are 0.3 μm for TEM, 10 μm for LM-FE-SEM, and 0.5 μm for HM-FE-SEM. Above the percolation threshold (~13 vol % PDMS−SiO_x) the formation of highly hierarchal roughness results in superhydrophobic nanocomposites.

similar to that of pure PS, which is consistent with XPS results. Above 13 vol % PDMS−SiO_x the DCA's increase, with a DCA $\approx 95°$ measured at 20% bulk PDMS−SiO_x. This implies a significant increase in both PDMS−SiO_x surface concentration ($\theta_l = 70°$ for diiodomethane on physisorbed PDMS),[16] which is again consistent with the XPS results, and an increase in surface roughness. AFM was used to probe the surface topography, and the resulting images, root-mean-square (rms) roughness values (σ), and ratios of the topographical area to the projected surface area (κ) as a function of PDMS−SiO_x loading are shown in Figure 3. Note that the sample preparation methods and thermal processing conditions used here resulted in < 1 nm rms roughness and $\kappa \approx 1$ for the pure PS−ND coating (no filler loading). The rms roughness (σ) results do not show any kind of obvious transition around 13 vol % PDMS−SiO_x, although the results do show power-law behavior over the range of 5−17 vol % filler, with a power-law exponent of 1.7. The values for κ show (i) a resistance to creation of surface area below 13 vol % PDMS−SiO_x and (ii) a significant increase in surface area from 13 to 17% PDMS−SiO_x which corresponds to the transition from hydrophobic to superhydrophobic, as shown in Figure 1a. The apparent decrease in σ and κ values from 17 to 20 vol % loading is primarily due to the inability of the AFM tip to probe the entire surface of the samples at 20 vol %. As will be shown with the FE-SEM images, the surface is highly fractal at the highest filler loading. The results in Figures 2 and 3 thus lead to an important question: What type of transition in the nanocomposite system could cause significantly enhanced nanoparticle surface segregation and roughening resulting in a sharp transition in surface hydrophobicity?

This question can be answered when the bulk nanocomposite morphologies and resolved details of the surface roughness hierarchy are considered. Figure 4 shows TEM images of the bulk nanocomposites, FE-SEM images resolving both microscale and nanoscale roughness of the nanocomposite surfaces, and the corresponding WCA's as a function of PDMS−SiO_x concentration. The sharp transition from hydrophobic to superhydrophobic corresponds to the bulk percolation threshold at 13 vol % filler, as approximated from the TEM images in Figure 4. This percolation threshold concentration is further supported (independently) by hardness tests performed on the annealed PS−ND nanocomposite coatings, as shown in Figure 5, with a comparison to the Halpin−Tsai model.[13] Hardness measurements were chosen to independently probe the percolation threshold because they provide quantitative analysis of mechanical reinforcement in polymer nanocomposites and do not require further processing of the coating samples (e.g., compression molding of bulk nanocomposites for dynamic mechanical analysis). The percolation threshold determined here is indeed consistent with previously reported results for similar systems.[25,26] Although

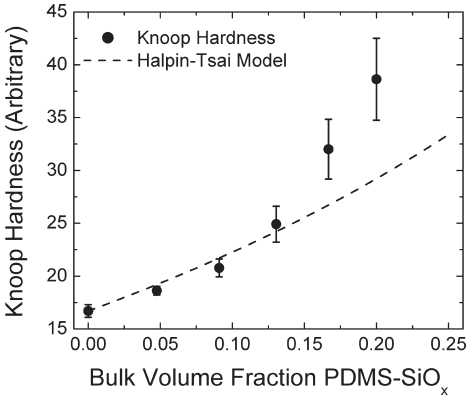

Figure 5. Knoop hardness results for annealed PS−ND nanocomposite coatings as compared to the Halpin−Tsai model. The deviation from the model predictions begins ~13 vol % PDMS−SiO_x, which supports the TEM-approximated percolation threshold.

percolation theoretically occurs at ~30 vol % loading for hard spheres in a noninteracting fluid,[27] it has been found to vary greatly depending on factors such as polymer/particle thermodynamic interactions, particle geometry, particle size and size distribution, and polymer molecular weight and polydispersity.[22,23] Here, the unfavorable interactions between the nanoparticles and the polymer matrix (γ_{pm} = 6 mJ/m^2)[21] as well as the long-range attractive van der Waals forces between particles[15,28] help to drive aggregation and percolation.

Percolation is well-known to cause dramatic changes in the rheological, mechanical (see Figure 5), and electrical properties of polymer nanocomposites due to long-range assembly of the nanoparticles.[23,25,29] Here, this long-range assembly promotes formation of multiscale roughness at the nanocomposite surfaces. Formation of surface defects (e.g., through cavitation) will also enhance superhydrophobicity of the nanocomposite coatings. Unfortunately, the rms roughness (σ) and κ values shown in Figure 3 do not provide details regarding the *distribution of characteristic roughness length scales*, which is a primary factor in controlling surface hydrophobicity through physical means (i.e., the Lotus effect).[2] However, the FE-SEM images shown in Figure 4 demonstrate that, above the percolation threshold, nanoscale roughness becomes more prominent and couples to the microscale roughness. Highly hierarchal topographies are clearly identifiable at 17 and 20% filler loadings, with corresponding WCA's of approximately 160 and 170°, respectively, and water roll-off at tilt angles $\ll$10°.

In conclusion, we have created thermally equilibrated superhydrophobic polymer nanocomposite coatings by forming highly hierarchal surfaces through percolation-driven surface segregation of the nanoparticles. Below the percolation threshold of the nanocomposites, superhydrophobicity was not achievable because the thermodynamic forces that drive hydrophobic nanoparticles to polymer surfaces during thermal annealing are not strong enough to create extensive surface roughening. However, above the percolation threshold multiscale roughness developed (i.e., the Lotus effect), thereby resulting in WCA's as high as 170° (see Figures 2 and 4) and roll-off at tilt angles $\ll$10°. Future work can use the principles outlined here to develop uniform superhydrophobic coatings of various chemistries, physical properties, and functionalities as well as superoleophobic coatings (e.g., through fluorination)[5] and even highly conductive coatings that are superamphiphobic (e.g., superhydrophobic or superoleophobic).

Acknowledgment. S.E.H. thanks Masahiko Ishii (Toyota Motor Corp., Toyota, Aichi, Japan) for supporting this project and Paul Fanson and Kazuaki Sato (Toyota Research Institute of North America, Ann Arbor, MI) for reviewing the manuscript. FE-SEM of the nanocomposite surfaces and TEM of the PDMS−SiO_x nanoparticles were performed at the Electron Microbeam Analysis Laboratory (EMAL) at the University of Michigan (Ann Arbor, MI). Microtomy and TEM of the bulk nanocomposites as well as AFM and XPS of the nanocomposite surfaces were performed by Evans Analytical Group (Sunnyvale, CA). Elemental analysis was performed by Galbraith Laboratories, Inc. (Knoxville, TN).

Supporting Information Available: Details of the materials used, sample preparation methods, experimental analysis, and derivation of eqs 2 and 3 are available. This material is available free of charge via the Internet at http://pubs.acs.org.

References and Notes

(1) Chaudhury, M. K.; Whitesides, G. M. *Science* **1992**, *256*, 1539–1541.
(2) Gao, L.; McCarthy, T. J. *Langmuir* **2009**, *25*, 14105–14115.
(3) Feng, X.; Jiang, L. *Adv. Mater.* **2006**, *18*, 3063–3078.
(4) Onda, T.; Shibuichi, S.; Satoh, N.; Tsujii, K. *Langmuir* **1996**, *12*, 2125–2127.
(5) Steele, A.; Bayer, I.; Loth, E. *Nano Lett.* **2009**, *9*, 501–505.
(6) Öner, D.; McCarthy, T. J. *Langmuir* **2000**, *16*, 7777–7782.
(7) Genzer, J.; Efimenko, K. *Science* **2000**, *290*, 2130–2133.
(8) Tuteja, A.; Wonjae, C.; Ma, M.; Mabry, J. M.; Mazella, S. A.; Rutledge, G. C.; McKinley, G. H.; Cohen, R. E. *Science* **2007**, *318*, 1618–1622.
(9) Zhai, L.; Cebeci, F. Ç.; Cohen, R. E.; Rubner, M. F. *Nano Lett.* **2004**, *4*, 1349–1353.
(10) Otten, A.; Herminghaus, S. *Langmuir* **2004**, *20*, 2405–2408.
(11) Boinovich, L.; Emelyanenko, A. *Langmuir* **2009**, *25*, 2907–2912.
(12) Yüce, M. Y.; Demirel, A. L.; Menzel, F. *Langmuir* **2005**, *21*, 5073–5078.
(13) Hub, C.; Harton, S. E.; Hunt, M. A.; Fink, R.; Ade, H. *J. Polym. Sci., Part B: Polym. Phys.* **2007**, *45*, 2270–2276.
(14) Soga, I.; Granick, S. *Macromolecules* **1998**, *31*, 5450–5455.
(15) Israelachvili, J. *Intermolecular & Surface Forces*; Academic Press: Burlington, MA, 2007.
(16) Owens, D. K.; Wendt, R. C. *J. Appl. Polym. Sci.* **1969**, *13*, 1741–1747.
(17) Wenzel, R. W. *Ind. Eng. Chem.* **1936**, *28*, 988–994.
(18) Cassie, A. G. D.; Baxter, S. *Trans. Faraday Soc.* **1944**, *40*, 546–551.
(19) Gao, L.; McCarthy, T. J. *Langmuir* **2007**, *23*, 3762–3765.
(20) Erbil, H. Y.; Cansoy, C. E. *Langmuir* **2009**, *25*, 14135–14145.
(21) Owen, M. J. Surface and Interfacial Properties. In *Physical Properties of Polymers Handbook*; Mark, J. E., Ed.; American Institute of Physics: Woodbury, NY, 1996; pp 669−676.
(22) Surve, M.; Pryamitsyn, V.; Ganesan, V. *Langmuir* **2006**, *22*, 969–981.
(23) Cassagnau, Ph. *Polymer* **2008**, *49*, 2183–2196.
(24) Dann, J. R. *J. Colloid Interface Sci.* **1970**, *32*, 302–320.
(25) Jouault, N.; Vallat, P.; Dalmas, F.; Said, S.; Jestin, J.; Boué, F. *Macromolecules* **2009**, *42*, 2031–2040.
(26) Bogoslovov, R. B.; Roland, C. M.; Ellis, A. R.; Randall, A. M.; Robertson, C. G. *Macromolecules* **2008**, *41*, 1289–1296.
(27) Sen, S.; Thomin, J. D.; Kumar, S. K.; Keblinski, P. *Macromolecules* **2007**, *40*, 4059–4067.
(28) Borukhov, I.; Leibler, L. *Macromolecules* **2002**, *35*, 5171–5182.
(29) Kota, A. K.; Cipriano, B. H.; Duesterberg, M. K.; Gershon, A. L.; Powell, D.; Raghavan, S. R.; Bruck, H. A. *Macromolecules* **2007**, *40*, 7400–7406.